Research Article | Vol. 25, No. 4 | 20 Feb 2017 | OPTICS EXPRESS 3927

Optics EXPRESS

Electrically pumped continuous wave quantum dot lasers epitaxially grown on patterned, on-axis (001) Si

JUSTIN NORMAN,[1,*] M. J. KENNEDY,[2] JENNIFER SELVIDGE,[1] QIANG LI,[3] YATING WAN,[3] ALAN Y. LIU,[1] PATRICK G. CALLAHAN,[1] MCLEAN P. ECHLIN,[1] TRESA M. POLLOCK,[1] KEI MAY LAU,[3] ARTHUR C. GOSSARD,[1] AND JOHN E. BOWERS[1,2]

[1]*Materials Department, University of California Santa Barbara, Santa Barbara, California, 93106, USA*
[2]*Department of Electrical and Computer Engineering, University of California Santa Barbara, Santa Barbara, California, 93106, USA*
[3]*Department of Electronic and Computer Engineering, Hong Kong University of Science and Technology, Clear Water Bay, Kowloon, Hong Kong, China*
[*]*jnorman@umail.ucsb.edu*

Abstract: High performance III-V lasers at datacom and telecom wavelengths on on-axis (001) Si are needed for scalable datacenter interconnect technologies. We demonstrate electrically injected quantum dot lasers grown on on-axis (001) Si patterned with {111} v-grooves lying in the [110] direction. No additional Ge buffers or substrate miscut was used. The active region consists of five InAs/InGaAs dot-in-a-well layers. We achieve continuous wave lasing with thresholds as low as 36 mA and operation up to 80°C.

OCIS codes: (140.5960) Semiconductor lasers; (230.5590) Quantum-well, -wire, and -dot devices.

References and links

1. Z. Zhou, B. Yin, and J. Michel, "On-chip light sources for silicon photonics," Light Sci. Appl. **4**(11), e358 (2015).
2. A. Y. Liu, C. Zhang, J. Norman, A. Snyder, D. Lubyshev, J. M. Fastenau, A. W. K. Liu, A. C. Gossard, and J. E. Bowers, "High performance continuous wave 1.3 μm quantum dot lasers on silicon," Appl. Phys. Lett. **104**(4), 041104 (2014).
3. A. Y. Liu, S. Srinivasan, J. Norman, A. C. Gossard, and J. E. Bowers, "Quantum dot lasers for silicon photonics," Photon. Reas. **3**(5), B1–B9 (2015).
4. A. Y. Liu, R. W. Herrick, O. Ueda, P. M. Petroff, A. C. Gossard, and J. E. Bowers, "Reliability of InAs/GaAs quantum dot lasers epitaxially grown on silicon," IEEE J. Sel. Top. Quantum Electron. **21**(6), 1900708 (2015).
5. S. Chen, W. Li, J. Wu, Q. Jiang, M. Tang, S. Shutts, S. N. Elliott, A. Sobiesierski, A. J. Seeds, I. Ross, P. M. Smowton, and H. Liu, "Electrically pumped continuous-wave III-V quantum dot lasers on silicon," Nat. Photonics **10**(5), 307–311 (2016).
6. A. Y. Liu, J. Peters, X. Huang, D. Jung, J. Norman, M. L. Lee, A. C. Gossard, and J. E. Bowers, "Electrically pumped continuous-wave 1.3 μm quantum-dot lasers epitaxially grown on on-axis (001) GaP/Si," Opt. Lett. **42**(2), 338–341 (2017).
7. D. Jung, A. Y. Liu, J. Peters, J. Norman, X. Huang, M. L. Lee, A. C. Gossard, and J. E. Bowers, "Electrically pumped continuous wave III-V quantum dot lasers epitaxially grown on exact GaP/Si (001)," presented at the International Conference on Molecular Beam Epitaxy, Montpellier, France, 4–9, Sept. 2016.
8. A. Y. Liu, J. Peters, D. Jung, X. Huang, J. Norman, M. L. Lee, A. C. Gossard, and J. E. Bowers, "InAs/GaAs quantum dot lasers on exact GaP/Si (001)," presented at the North American Conference on Molecular Beam Epitaxy, Saratoga Springs, New York, 18–21, Sept. 2016.
9. Q. Li, K. W. Ng, and K. M. Lau, "Growing antiphase-domain-free GaAs thin films out of highly ordered planar nanowire arrays on exact (001) silicon," Appl. Phys. Lett. **106**(7), 072105 (2015).
10. M. Paladugu, C. Merckling, R. Loo, O. Richard, H. Bender, J. Dekoster, W. Vandervorst, M. Caymax, and M. Heyns, "Site selective integration of III-V materials on Si for nanoscale logic and photonic devices," Cryst. Growth Des. **12**(10), 4696–4702 (2012).
11. Q. Li, Y. Wan, A. Y. Liu, A. C. Gossard, J. E. Bowers, E. L. Hu, and K. M. Lau, "1.3-μm InAs quantum-dot micro-disk lasers on V-groove patterned and unpatterned (001) silicon," Opt. Express **24**(18), 21038–21045 (2016).

#282133 https://doi.org/10.1364/OE.25.003927
Journal © 2017 Received 6 Dec 2016; revised 8 Feb 2017; accepted 9 Feb 2017; published 14 Feb 2017

Optics EXPRESS

12. Y. Wan, Q. Li, A. Y. Liu, A. C. Gossard, J. E. Bowers, E. L. Hu, and K. M. Lau, "Optically pumped 1.3 μm room-temperature InAs quantum-dot micro-disk lasers directly grown on (001) silicon," Opt. Lett. **41**(7), 1664–1667 (2016).
13. Y. Wan, Q. Li, A. Y. Liu, W. W. Chow, A. C. Gossard, J. E. Bowers, E. L. Hu, and K. M. Lau, "Sub-wavelength InAs quantum dot micro-disk lasers epitaxially grown on exact Si (001) substrates," Appl. Phys. Lett. **108**(22), 221101 (2016).
14. Z. Wang, B. Tian, M. Pantouvaki, W. Guo, P. Absil, J. V. Campenhout, C. Merckling, and D. V. Thourhout, "Room-temperature InP distributed feedback laser array directly grown on silicon," Nat. Photonics **9**(12), 837–842 (2015).
15. G. Kurczveil, D. Liang, M. Fiorentino, and R. G. Beausoleil, "Robust hybrid quantum dot laser for integrated silicon photonics," Opt. Express **24**(14), 16167–16174 (2016).

1. Introduction

As bandwidth consumption continues to rapidly increase globally, so too does the need for downscaling optical interconnect technologies to meet the need for high bandwidth densities within the datacenter. Silicon photonics has proven itself in technoeconomic viability as a solution to interconnect downscaling [1]; however, there remains considerable room for improvement by obviating the need for heterogeneously integrated III-V light sources that increase chip cost through the high cost and limited scalability of native III-V substrates and the increased complexity of chip-scale bonding processes. Epitaxial integration of III-V lasers on silicon represents an alternative that eliminates the native substrate cost and, if integrated as a front-end process on a silicon-on-insulator (SOI) wafer, eliminates the need for bonding.

Due to their tolerance to the inherent crystalline defects of mismatched epitaxy, quantum dot lasers have shown promise for producing high performance lasers on silicon with low thresholds, long lifetimes, and continuous wave operation up to 119°C [2–5]. Unfortunately, previous results have all utilized miscut silicon substrates for their ability to avoid antiphase domain (APD) formation that results from polar/non-polar growth. Miscut substrates are not compatible with CMOS processing—the underlying basis of the economic viability of silicon photonics—and as such a solution for growth on on-axis (001) silicon is needed. The following presents an approach for epitaxial III-V lasers on on-axis silicon that uses a v-groove silicon template showing, in conjunction with our simultaneously developed GaP/Si template [6–8], the first reported demonstration of room temperature (RT) continuous wave (CW) operation.

Our approach uses selective patterning of an on-axis (001) silicon substrate to simultaneously circumvent the issue of antiphase domains and reduce the dislocation density in a coalesced GaAs buffer layer that forms the substrate for laser regrowth. This GaAs-on-v-groove-silicon (GoVS) [9] and analogous InP-on-v-groove-silicon template [10] has been demonstrated to suppress APD formation and filter dislocations and stacking faults. The GoVS template has been used for optically pumped microdisk lasers on silicon down to the submicron level [11–13]. Using InP as the III-V material, optically pumped, epitaxial DFB lasers have been demonstrated [14]. Using the GoVS template, we report here electrically injected, Fabry-Perot, quantum dot ridge lasers showing CW operation up to 80°C with threshold currents as low as 37 mA.

2. Experimental methods

N-type on-axis (001) silicon substrates were used for the lasers. The silicon substrates were prepared according to the methods presented in [11]. The silicon was initially patterned with 90 nm wide stripes of SiO_2 with 40 nm spacing using standard dry etching techniques. After patterning, the substrates were subjected to an RCA-1 clean and a brief 1% HF dip to remove the native oxide before immediately etching the v-grooves. The v-grooves were etched using a 45% KOH solution at 70°C for 15 s. The KOH solution etches anisotropically with a high selectivity for the {111} crystal planes.

The growth of the GaAs-on-v-groove Si template was performed in a low-pressure (100 mbar) metal-organic chemical deposition (MOCVD) system with a horizontal reactor

Optics EXPRESS

(AIXTRON 200/4). Triethylgallium (TEGa), Trimethylgallium (TMGa), and Trimethylaluminum (TMAl) were used as group III precursors, while Tertiarybutylarsine (TBA) was used as the Group V precursor. The patterned Si substrate was thermally cleaned in the MOCVD chamber at 800°C for 15 min in an H_2 ambient. Selective area heteroepitaxy of GaAs nanowires was conducted with parameters detailed in [9]. After removing the SiO_2 stripes using buffered oxide etch (BOE), the GaAs nanowires were coalesced into a 1 µm continuous thin film at 600°C with stepped growth rates from 8 nm/min to 32 nm/min. This is followed by ten periods of an $Al_{0.3}Ga_{0.7}As$/GaAs (10 nm/ 8 nm) superlattice and finally 800 nm of GaAs grown at 700°C. The GaAs growth was performed at V/III ratios ranging from 5 to 20. The insertion of the superlattice greatly smoothened the surface of the GoVS template. An AFM scan across an area of 10 × 10 μm^2 revealed a root-mean-square roughness of 0.9 nm. Analysis from XRD x-rocking curves yielded a full-width-at-half-maximum value of 140 arcsec, indicating the good crystalline quality.

Molecular beam epitaxy (MBE) was used to grow the laser structure. Prior to regrowth, the samples were cleaned with solvents and a dilute HF dip. The samples were grown using a Veeco Gen II MBE system. Growth was initiated with the n-contact layer and no additional buffer layers. The epi structure consisted of five InAs quantum dot layers in $In_{0.15}Ga_{0.85}As$ quantum wells clad in a GaAs/AlGaAs graded-index separate-confinement heterostructure for optical and electrical confinement. The active dot-in-a-well layers were grown at 495°C under As_4 overpressure with V/III ratios of 10, 35, and 35 for the 2 nm InGaAs prelayer, InAs quantum dots, and 5 nm InGaAs cap, respectively. The nominal InAs thickness was 2.75 ML. Following the deposition of each active layer, a 2.5 nm GaAs layer was deposited at 495°C, and the substrate temperature was increased to 580°C for a five minute anneal to evaporate oversized defective dots and truncate the overall size distribution for increased uniformity. Cladding and contact layers were grown at 580°C. A full schematic of the epitaxial structure is shown in Fig. 1.

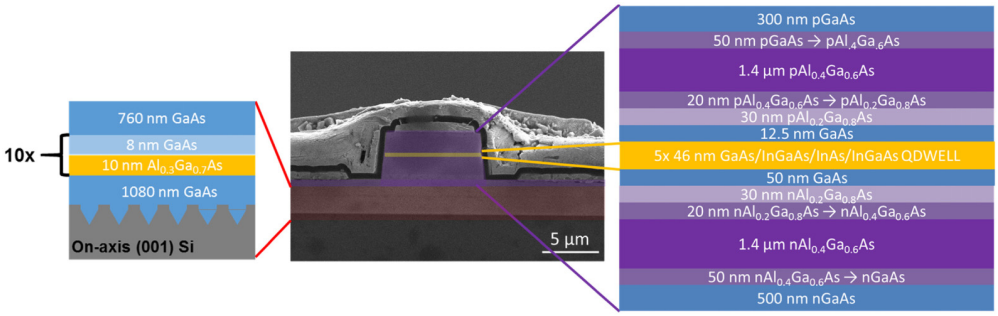

Fig. 1. Scanning electron microscope image of a polished facet with false color indicating the various sections of the device.

The laser material was processed into deeply-etched ridge lasers with ridge running perpendicular to the v-grooves, using standard dry etching and deposition techniques, with cavity lengths of 800, 1000, and 1200 µm and ridge widths ranging from 4 to 12 µm. Pd/Ti/Pd/Au and Pd/Ge/Au metallizations were used for the p- and n-contacts respectively. The n-contact was probed from laterally displaced pads while the p-contact was injected from the top of the ridge as depicted in Fig. 2. Laser facets were formed by dicing and polishing. A subset of the devices later had a 95% high reflectivity coating applied to one facet for high temperature measurement. A scanning electron microscope image of the cleaved cross-section and a top-down optical micrograph of the finished devices are shown in Fig. 1 and Fig. 2 respectively.

Optics EXPRESS

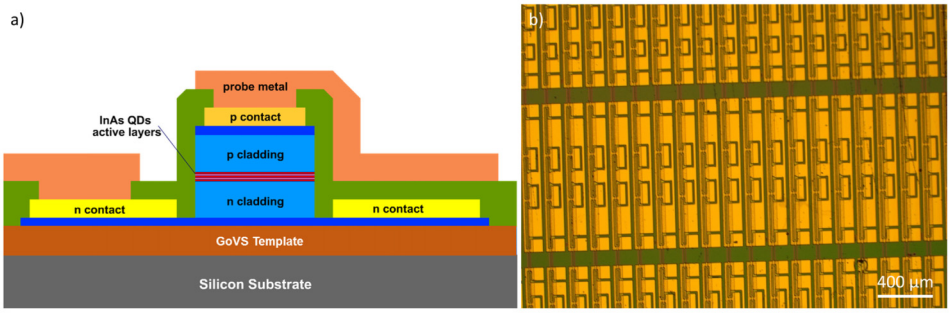

Fig. 2. (a) A schematic cross-section of the fabricated devices. (b) Top-down optical micrograph of the fabricated ridge lasers before dicing.

3. Results and discussion

The as-grown GoVS template material quality was assessed through electron channeling contrast imaging (ECCI). This technique uses a scanning electron microscope in backscatter mode at a given diffraction condition to image deviations from the Bragg condition caused by strain fields such as those around dislocations and local phase shifts of the electron wave caused by the non-integer lattice translations across stacking faults. ECCI allows for rapid acquisition of large area scans without any material preparation making it advantageous over transmission electron microscopy for obtaining accurate defect densities in low defect density materials. Figure 3 displays a scan of a GoVS template comparable to the design used for laser regrowth. In the image, the lines and pinpoints of bright contrast respectively indicate stacking faults and threading dislocations intersecting the surface. By counting the defects, densities of $7\text{x}10^7$ cm^{-2} and $2\text{x}10^7$ cm^{-2} were calculated for threading dislocations and stacking faults respectively. The threading dislocation density compares favorably with our previous work on miscut GaAs/Ge/Si in [2]. It is reasonable to expect this defect density to be comparable to if slightly larger than what would be measured in the laser's active layers as there are no additional strained layers between the as-grown GoVS template and the quantum dot layers.

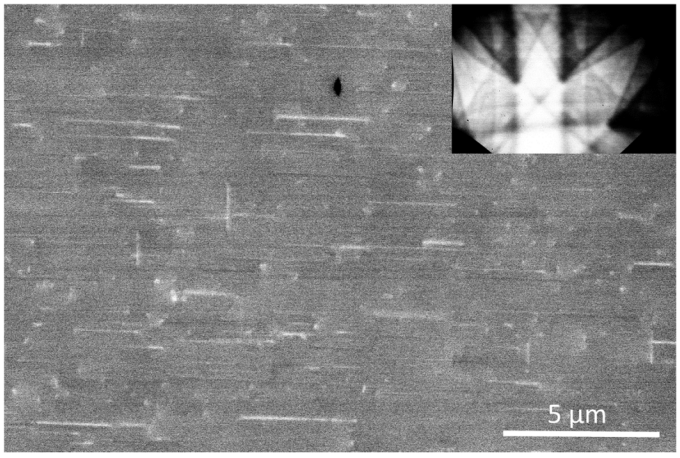

Fig. 3. Plan-view electron channeling contrast image (ECCI) of a GaAs-on-v-groove-Si template. The bright dashes are attributed to stacking faults while the pinpoints represent threading dislocations intersecting the sample surface. Counting reveals a threading dislocation density of $7\text{x}10^7$ cm^{-2} and a stacking fault density of $2\text{x}10^7$ cm^{-2}. (Inset) The electron channeling pattern corresponding to the $(\bar{2}20)$ and $(0\bar{2}0)$ imaging condition used.

Optics EXPRESS

The optical quality of the quantum dots was assessed through the growth of photoluminescence (PL) structures on native GaAs substrates containing one embedded layer of quantum dots and one surface layer for atomic force microscopy (AFM) measurement of the dot density. The dots in the PL structures were grown with identical conditions to those used in the laser. The AFM and photoluminescence results are shown in Fig. 4. From the AFM scan a dot density of $6x10^{10}$ cm^{-2} can be estimated while the PL shows strong luminescence at 1277 nm with a full-width at half-maximum of 36 meV. It is expected that these results would largely transfer to growth on the GoVS template with a modest blue shift and slight broadening due to the effects of residual strain and increased surface roughness relative to native substrates. Unfortunately additional GoVS templates were not available at the time for a comparison of exactly identical structures which along with a comparison to other silicon-based templates is the subject of ongoing investigation.

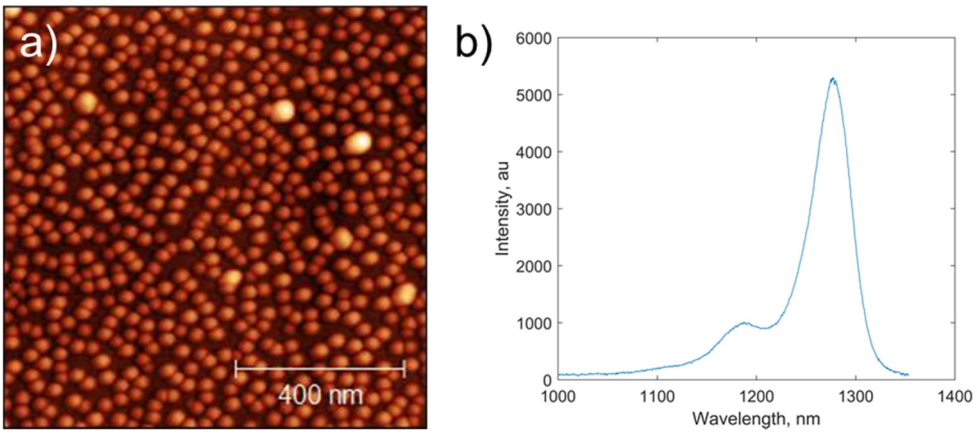

Fig. 4. (a) Atomic force microscope image of a 1x1 μm^2 region of quantum dots showing a total dot density of $6x10^{10}$ cm^{-2}. (b) A photoluminescence spectrum for the quantum dots grown on a native GaAs substrate with conditions identical to those used for the laser showing a peak wavelength of 1277 nm and full-width at half-maximum of 36 meV.

Approximately 200 ridge lasers were fabricated and tested at room temperature in CW operation. Figure 5(a) displays representative single-side light output and voltage versus injection current curves for a 9x1200 μm^2 device showing a clear threshold at 81 mA and single-side output power over 50 mW. The I-V curve indicates a relatively low series resistance of 2-3 Ω. Figure 5(b) shows the lasing spectrum of the same device indicating ground state lasing initially at 1250 nm and shifting to 1257 and 1270 nm as it picks up supermodulation that is attributed to lasing from higher order transverse modes and is consistent with previous observations [5]. Higher resolution scans show side lobes on the Fabry-Perot ripples further adding support to simultaneous lasing from orthogonal transverse modes. Excited state lasing is not observed prior to the thermal rollover point at 700 mA.

Optics EXPRESS

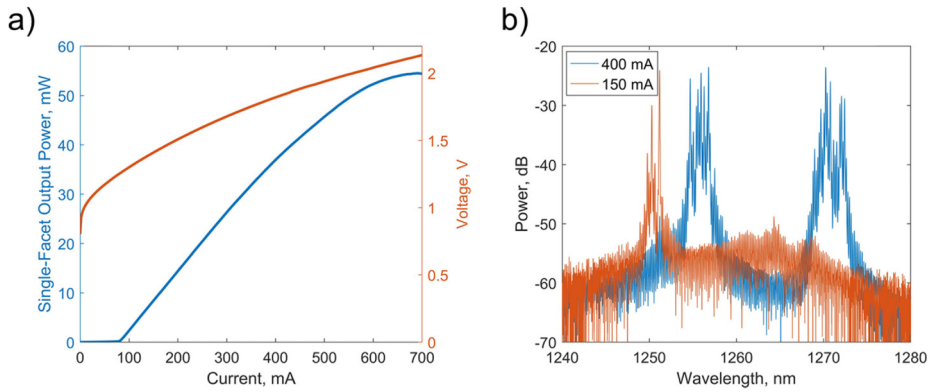

Fig. 5. (a) Continuous wave light output and voltage as a function of the injection current of a 9x1200 µm2 device showing a threshold of 81 mA and maximum single-side output power of 55 mW. (b) The above threshold optical spectrum showing ground state lasing near 1250 nm which transitions to dual lasing attributed to multimode lasing from higher order transverse modes. Excited state lasing was not observed for the given injection levels.

A full depiction of the measurement data is presented in Fig. 6. Figure 6(a) shows the absolute thresholds of 183 lasers with polished facets broken down by the ridge width and cavity length. There is a clear trend of higher thresholds with wider ridges as would be expected, but there is an unexpected dip for the wider ridges at 10 and 11 µm. This discrepancy is attributed to facet damage during polishing which is potentially less severe for the lower aspect ratio ridges. Figure 6(b) shows a histogram of the threshold current density broken down by cavity length showing a minimum value of 498 A/cm^2. Similar devices on miscut Ge/Si substrates showed thresholds current densities down to 200 A/cm^2 [2] indicating room for improvement through further optimization of the GoVS template design and growth conditions. The high threshold tail of the distributions is attributed to the yield of mechanical facet polishing. Figure 6(c) and 6(d) show the light output characteristics of the lasers through the maximum ground state output power and the differential quantum efficiency (DQE)—calculated using the central wavelength of 1260 nm from Fig. 5(b) and assuming equal output from both facets. The assumption of equal output could be violated if facet damage during polishing is not similar for both facets. In this case device output power and DQE could be larger as-measured due to only collecting light output from one facet. Devices of all sizes routinely put out a few tens of milliwatts of output power with the maximum single-side output power of 84 mW being achieved by a 10x1200 µm^2 ridge. The threshold current of this device was 73 mA (607 A/cm^2) which is comparable to other ridges of the same size indicating that the high output power is likely not erroneous due to facet damage. Most of the measured values for the DQE fall within the range of 0.15-0.30 which is similar to values obtained in our previous devices on miscut Ge/Si [2] and is roughly half of the value of 0.50 that we have obtained on cleaved broad area lasers on native GaAs substrates (data not shown). Again the spread in data at a given geometry is attributed to facet polishing yield which, in the case of DQE, can lead to erroneously large and small measurements. The 8x1200 µm^2 device that yielded a DQE of 0.40 had a threshold of 100 mA (1038 A/cm^2) indicating that it is on the upper end of the interquartile range for that device geometry suggesting that the measurement could be influenced by facet damage.

Optics EXPRESS

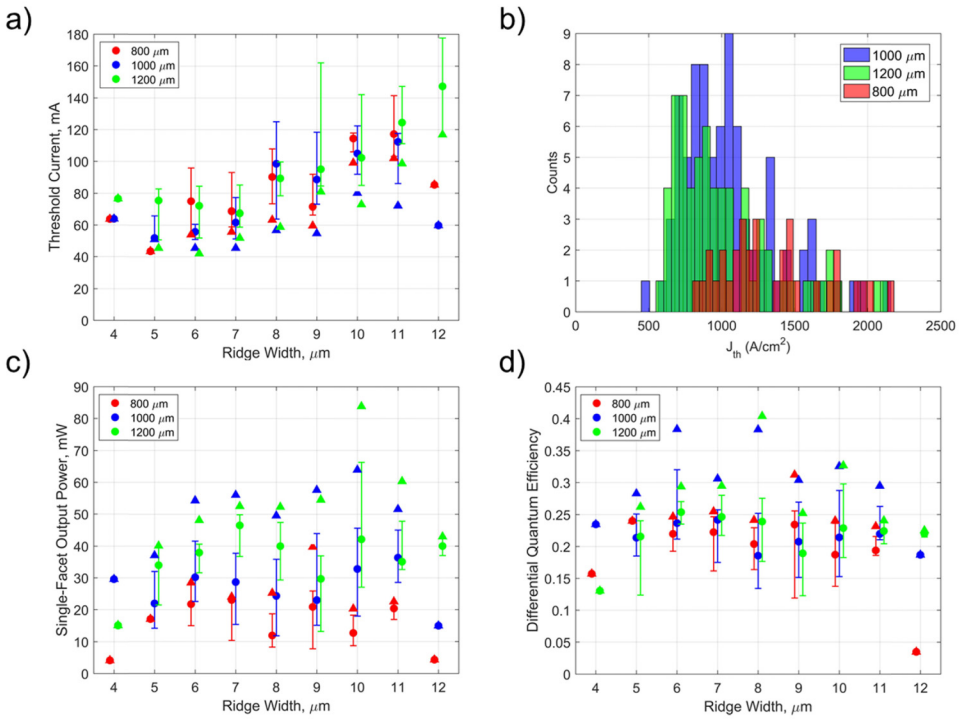

Fig. 6. The aggregation of laser performance figures of merit is presented. For clarity data from different cavity lengths has been shifted in the scatter plots to the left or right about a given ridge width. Error bars indicate the interquartile range of device performance, circular data points indicate the median peroformance, and triangles designate the best measurement for each cavity size. (a) Threshold current for all lasers of varying ridge width and length is plotted. (b) Threshold current density is plotted for all devices as a histogram showing peaked distribution around 700-1000 A/cm^2 and a minimum value of 498 A/cm^2. (c) The single-side peak output power (ground state lasing only) is plotted for according to geometry for all devices with a peak value of 84 mW. (d) The differential quantum efficiency is plotted for all devices calculated using the central wavelength of 1260 nm from Fig. 5(b) with a maximum value of 40%.

A subset of the previous devices was coated on one facet with a 95% reflectivity coating using Ta_2O_5/SiO_2 quarter wavelength distributed Bragg reflectors. Unfortunately, most of the devices were damaged during preparation for the coating deposition. From the devices that survived, a minimum threshold current of 36 mA was achieved with a 6x1200 μm^2 ridge.

Realistic datacenter environments operate at elevated temperatures, so prospective laser technologies must be able to function in these environments under CW operation with minimal cooling. To test the high temperature performance of our devices, we placed an 8x1200 μm^2 ridge with one HR coated facet on a heated stage and measured the LI curves at elevated temperatures. The room temperature threshold current and maximum output power for this device were 40 mA and 93 mW respectively. The results are plotted in Fig. 7. A clear threshold is observed in each measurement over the temperature range from 20 to 80°C. This result matches that of our lasers on GaP/Si templates for ground state lasing [6–8] (note that the 90°C result in [6–8] was from the excited state) despite the reduced number of active layers (five versus seven) and lack of modulation p-doping in the current structure. These results with those of [6–8] represent the highest demonstrated O-band CW lasing temperature of any epitaxial laser grown directly on silicon (without Ge), miscut or otherwise, and compare favorably to the best heterogeneously integrated quantum dot lasers on Si which operate CW up to 100°C [15].

Optics EXPRESS

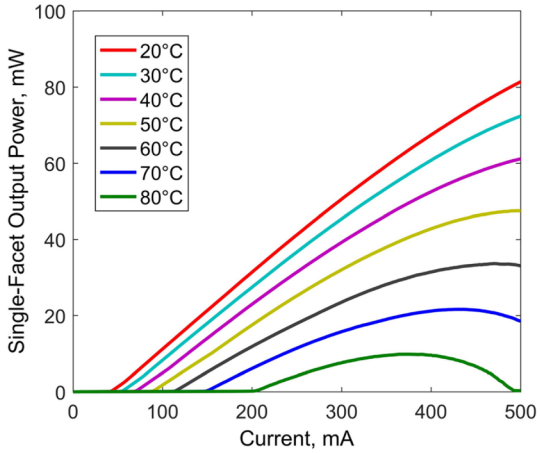

Fig. 7. Continuous wave light output power as a function of injection current for a 8x1200 μm^2 device with one polished facet and one 95% high reflection coated facet at temperatures from 20 to 80°C.

4. Conclusion

We have demonstrated the first electrically pumped continuous wave operation of a III-V laser on a patterned on-axis silicon substrate with no Ge buffer layer. Deeply-etched ridge waveguide lasers were fabricated demonstrating threshold currents as low as 36 mA (6x1200 μm^2), single-side output powers up to 84 mW (10x1200 μm^2), and continuous wave ground state lasing up to 80°C (8x1200 μm^2 with HR coating). This work represents a significant step toward the compatibility of high performance III-V lasers with the industrial scale fabrication infrastructure of silicon photonics and CMOS foundries.

Funding

Air Force Research Laboratory (AFRL) (FA8650-15-2-5220); Advanced Research Projects Agency-Energy (ARPA-E) (DE-AR0000672); Research Grants Council of Hong Kong (RGC) (No 16212115); Innovation Technology Fund of Hong Kong (ITS/320/14); National Science Foundation Graduate Research Fellowship Program (NSFGRFP).

Acknowledgments

We are grateful to Kurt Olsson and John English for their assistance in MBE maintenance and Chris Palmstrom for fruitful discussions.